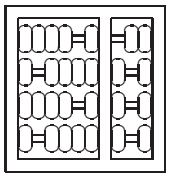

INSTITUTO DE COMPUTAÇÃO
UNIVERSIDADE ESTADUAL DE CAMPINAS

Automatic Extraction of Euclidean Isosurfaces for Visualization of Dysplastic Lesions from Brain MRI

F. P. G. Bergo *A. X. Falcão*
M. A. Montenegro *F. Cendes*

Technical Report - IC-05-08 - Relatório Técnico

May - 2005 - Maio

Automatic Extraction of Euclidean Isosurfaces for Visualization of Dysplastic Lesions from Brain MRI

Felipe P.G. Bergo[1] Alexandre X. Falcão[1] Maria Augusta Montenegro[2]
Fernando Cendes[2]
[1] Institute of Computing, State University of Campinas, Brazil
C.P. 6176 CEP 13084-971 Campinas - SP - Brazil
{felipe.bergo,afalcao}@ic.unicamp.br
[2] Department of Neurology, State University of Campinas, Brazil
guga@fcm.unicamp.br, fcendes@unicamp.br

Abstract

Curvilinear reformatting of MR images has been very useful in epilepsy research for detecting dysplastic lesions in the human brain. However, the method requires careful manual delineation and introduces artifacts. We present a fully automated approach to extract an "envelope" of the brain and obtain surfaces of same Euclidean distance to the envelope. The visualization of the voxel intensities on these isosurfaces substitute the previous procedure, eliminating its artifacts. The new approach was successfully evaluated over 40 controls and 10 patients with dysplastic lesions.

1 Introduction

The diagnosis of dysplastic cortical lesions is more effective when brain MR images are visualized using a curvilinear reformatting [1]. This procedure requires careful manual delineation of lines, following the curvature of the brain in several slices, and interpolation of their shape, for each patient [2]. The results are sensitive to manual delineation and the interpolation introduces curvature artifacts on the frontal and occipital lobes. In this work, we propose a fully automatic solution based on the image foresting transform (IFT) [3] and morphological operations [4]. The method extracts an "envelope" of the human brain from MR images and obtains surfaces of same Euclidean distance to the envelope. These isosurfaces are orthogonal to most of the sulci, enhancing the visualization of dysplastic lesions when the voxel intensities are mapped onto them.

2 Background

2.1 Dysplastic Lesions

Epilepsy is a frequent disorder characterized by recurrent seizures. About 15% of the patients have refractory seizures that cannot be controlled with medication. Focal cortical

dysplasia is one of the most frequent causes of refractory epilepsy, especially in childhood. It can be identified on MR images as focal cortical thickening, abnormal gyration and blurring between gray and white matter, often associated with clusters of heterotopic neurons [1]. The diagnosis of focal cortical dysplastic lesions is crucial for treatment planning, which generally involves surgical removal of the lesion.

2.2 The Image Foresting Transform

The IFT [3] is a framework for the design, implementation and evaluation of image processing operators. It is essentially a multiple-source extension of Dijkstra's algorithm [5] for more general *path-cost functions*, computed over a graph whose nodes are the voxels and whose arcs are implicitly defined by an *adjacency relation* between voxels. The IFT assigns one optimum path from a root set to each voxel, forming a minimum-cost path forest. The choice of roots, path-cost function and adjacency relation defines the image operator being implemented. It has been successfully used to compute watershed transforms [6, 7, 8, 9], fuzzy-connected object definition [10, 9], skeletonization and distance transforms [11], among other applications. The present work extends *tree-pruning* segmentation [12], a recent IFT-based method that exploits the topology of the forest to detect objects.

3 Methods

In tree pruning [12], a minimum-cost path forest is computed from a set of object voxels (internal markers). The markers become roots of the forest, represented in a predecessor map, where each voxel can reach its root by following the predecessor voxels in its optimum path. The key idea is that a suitable path-cost function should cause all paths that reach the background to cross the object's border through a few "weaker voxels", called *leaking points*. The object should be the remaining forest after removing the subtrees rooted at a voxel (pruning point) whose predecessor is a leaking point. This condition can be achieved with the f_{peak} path-cost function (the cost of a path is the maximum voxel intensity along that path) over a gradient intensity image and FIFO tie-breaking policy for voxels reached by two or more paths of same minimum cost [3]. The method assumes that, in real images – subject to noise and artifacts – object borders are not homogeneous and are very likely to have a few voxels with lower gradient values (leaking points).

Even though the above setting leads to a watershed transform [3, 7, 8, 9] when there are external markers, we are not interested in the watershed lines, but rather in the topology of the forest computed with only internal markers to identify the leaking points. To segment the brain by tree pruning, we need to I) extract internal markers; II) compute a suitable gradient intensity image; III) compute a minimum-cost path forest using the IFT operator with f_{peak} and IV) locate a set of leaking points in the forest. The methods for step III are covered in works by Falcão and others [3, 9]. We now present the details of acquisition and preprocessing, and then steps I, II and IV.

3.1 Image Acquisition and Preprocessing

All volumes used on this work were acquired in an Elscint 2T MR scanner, T1 gradient echo with sagittal slices. Pixels are 0.98×0.98 mm and slice thickness was either 1.0 or $1.5mm$. All volumes were interpolated to an isotropic voxel size of $0.98^3 mm$, and all further operations were performed on the isotropic datasets.

3.2 Marker Extraction

To extract a set of markers inside the brain, we exploit the fact that the brain is the largest connected object with intensities above a certain threshold. The intensity distribution varies among the datasets, but all images present a large peak at the low intensities (air and bone), and a large plateau of CSF, GM and WM[1] intensities. The marker extraction algorithm is presented below. Throughout this paper, we will use the notation $\mathcal{S}_k$ to denote a spherical structuring element of radius k for morphological operations.

Input: Image I
Output: Binary Marker Image B
1. Compute μ_P, the mean intensity of all voxels whose values are above 150.
2. Compute a binary image M by setting voxels of I with values above μ_P.
3. $M' \leftarrow M \ominus \mathcal{S}_3$.
4. $M'' \leftarrow$ largest connected component of M'.
5. $B \leftarrow M'' \ominus \mathcal{S}_4$.

The parameter μ_P represents the center of the CSF+GM+WM plateau, and it is safe to assume that voxels with intensity above μ_P are either within the dura-mater or are small components of vessels, muscle or noise. The erosion in line 3 ensures that skin and muscles are disconnected from the brain tissue. The selection of the largest connected component (line 4) excludes vessels and small components outside the brain. The erosion in line 5 reduces the marker set to avoid voxels outside the brain.

3.3 Gradient Intensity Computation

We want to enhance the border of the dura-mater, which has a smooth surface orthogonal to most of the sulci. This is done by computing, for each voxel, the standard deviation (σ) of the adjacent voxel values within a sphere of radius 3. This occurs due to the presence of 3 tissues close to the dura-mater (bone, CSF and GM), while keeping the GM/CSF border darker. To prevent background noise from creating false borders (since noise also leads to higher σ), the gradient intensity is set to zero on voxels with intensities below $0.25\mu_P$. A morphological erosion by $\mathcal{S}_1$ was applied to the gradient to weaken the bone-skin border, which would otherwise provide misleading leaking points along it.

[1] Cerebrospinal Fluid, Gray Matter and White Matter, respectively.

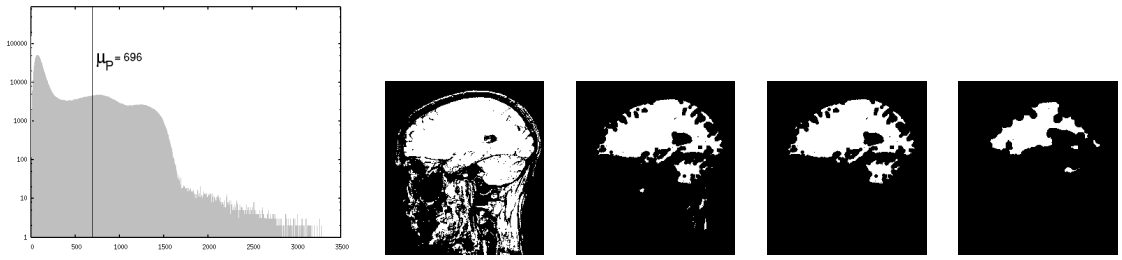

(a) (b) (c) (d) (e)

Figure 1: Marker extraction algorithm: (a) a log-scale plot of the input image histogram, showing the computed mean value, μ_P, of the plateau. Slices of the intermediary binary images, (b) M, (c) M', (d) M'', and (e) of the resulting marker image B.

3.4 Determination of Leaking Points

Given a predecessor map, it is possible to compute the number of descendants of each voxel in the forest. Since all paths that reach the background pass through the leaking points, the object voxels in the leaking paths present a higher number of descendants as compared to other voxels and, due to the FIFO policy, this number is considerably reduced for background voxels [12].

For brain MR volumes, we can safely assume that voxels on the volume's frame are background voxels. We compute, for each voxel, the number of descendants in the volume's frame. In this case, the sum of this number at the leaking points is the size $|F|$ of the frame. We also assume that the leaking point is the first voxel in the way back to the root with maximum number of descendants (except the root, whose predecessor is *nil*). This method is more robust than the one proposed by Falcão et al [12], since it is independent of thresholds. The algorithm is presented below.

Input: Predecessor map P, Set of frame voxels F.
Auxiliary: Descendant count map D, initially set to zero.
Output: Set of leaking points K
1. For each $v \in F$
2. While $v \neq nil$
3. $D(v) \leftarrow D(v) + 1$.
4. $v \leftarrow P(v)$.
5. $sz \leftarrow 0$.
6. For each $v \in F$ and while $sz \neq |F|$
7. max $\leftarrow -1$.
8. While $v \neq nil$
9. If $D(v) >$ max and $P(v) \neq nil$ Then
10. max $\leftarrow D(v)$ and $v_{\max} \leftarrow v$.
11. $v \leftarrow P(v)$.
12. If $v_{\max} \notin K$ Then $sz \leftarrow sz + D(v_{\max})$ and $K \leftarrow K \cup v_{\max}$.

Lines 1–4 compute, for each voxel v, the number $D(v)$ of descendants in the volume's frame. Lines 5–12 identify and insert in K the leaking points, $v_{\max}$, by the aforementioned method. The process halts when the sum of descendants sz of the points in K is equal to $|F|$.

3.5 Morphological Closing

Due to the inherent inhomogeneities of MR images, the segmentations obtained with the presented method alternate between the dura-mater and the cortex. We want an "envelope" as close as possible to the surface of the dura-mater, which leads to Euclidean isosurfaces that are orthogonal to most of the sulci. To solve this, we apply a morphological binary closing by $\mathcal{S}_{20}$ to the segmentation result, closing the sulci (Fig. 2).

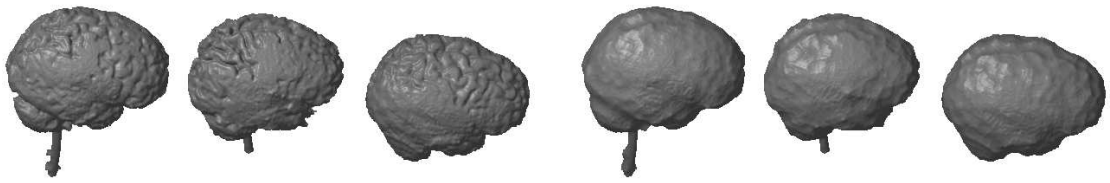

(a) (b)

Figure 2: Segmentation examples. (a) Before morphological closing; (b) The same three control volumes after the morphological closing.

3.6 Computation of Euclidean Isosurfaces

Once the envelope of the brain has been extracted, the isosurfaces can be obtained by a 3D Euclidean distance transform [13, 14] (Fig. 3), stored as a distance map, and visualized for any given distance threshold (depth from the envelope). This distance map can also be efficiently computed using an IFT where the roots are the voxels of the envelope (object border), the adjacency relation is given by $\mathcal{S}_{\sqrt{3}}$, and the cost of a path from a root to a voxel is the Euclidean distance between them [11]. This computation is also restricted to the interior of the envelope.

4 Results

We evaluated the method using 50 MR volumes, acquired and preprocessed as described in Section 3.1: 40 volumes were from control subjects with no known anomalies, and 10 volumes were from epilepsy patients (7 of these patients had dysplastic lesions confirmed by histological analysis of the tissue after surgery).

All volumes were successfully segmented using the proposed method. The interpolated volumes had from 136 to 192 slices of 256×256 pixels each. A 3.0 GHz Pentium-4 PC took 78 minutes to perform the 50 segmentations. The duration was mainly dependent of the

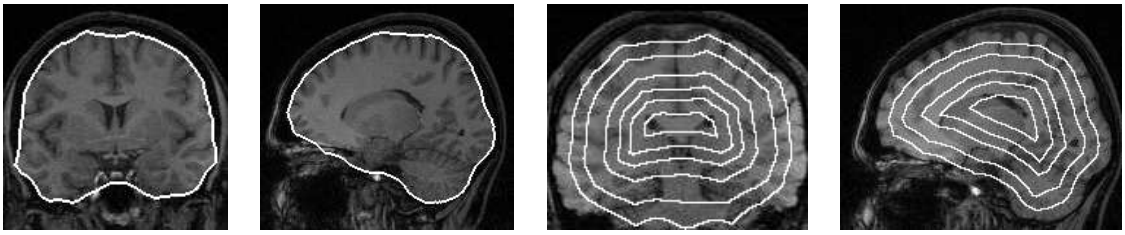

(a) (b) (c) (d)

Figure 3: Slices of Euclidean isosurfaces. Envelope in (a) coronal and (b) sagittal slices. Isosurfaces in (c) coronal and (d) sagittal slices.

gradient computation, which took about 35 seconds per volume. Fig. 4 shows 3D renditions of the resulting segmentations of the 50 volumes. Although the method does not provide a perfect segmentation of the brain, the inaccuracies near the extra-ocular muscles (Fig. 4, 10th column, 3rd row) and near the cerebellum (Fig. 4, 7th column, 3rd row) do not affect the visualization of the Euclidean isosurfaces for the purpose of dysplastic lesion detection, since they are still orthogonal to most of the sulci (Fig. 5).

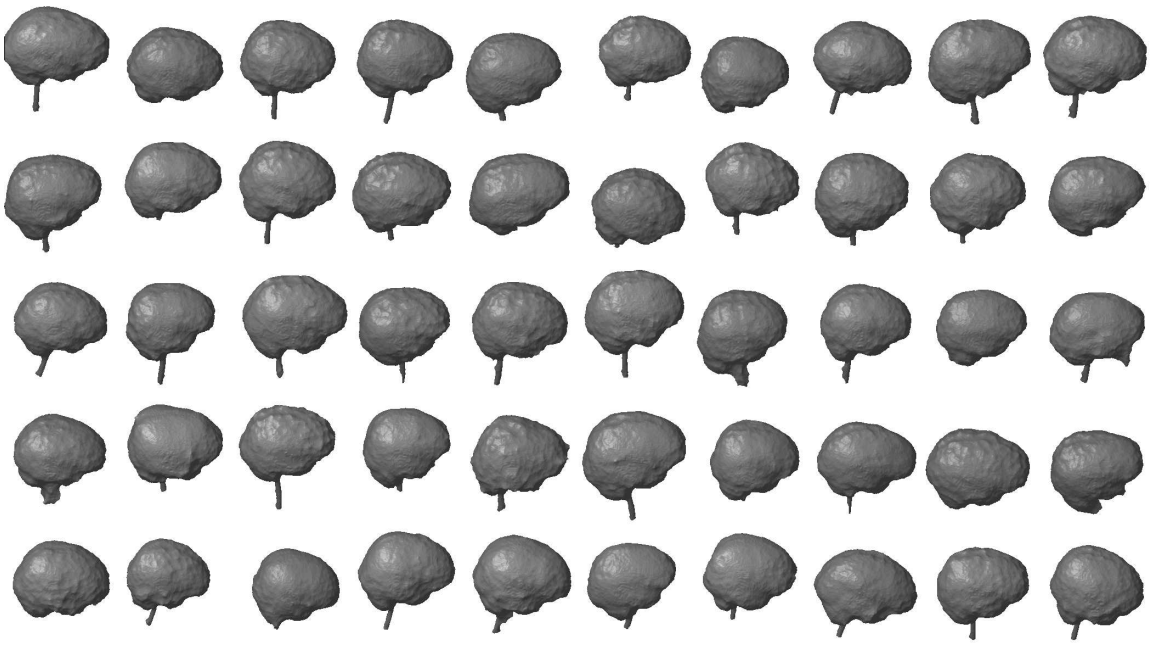

Figure 4: 3D renditions of the 50 envelopes. The four rows at the top are from the control subjects and the bottom row is from the epilepsy patients.

Fig. 5 shows some 3D renditions of the isosurfaces computed with the Alberio [15] software package, where the voxel intensities are mapped onto the surface. Alberio uses

the Euclidean IFT to compute the isosurfaces in about 9 seconds per volume on a 3.0 GHz Pentium-4 PC.

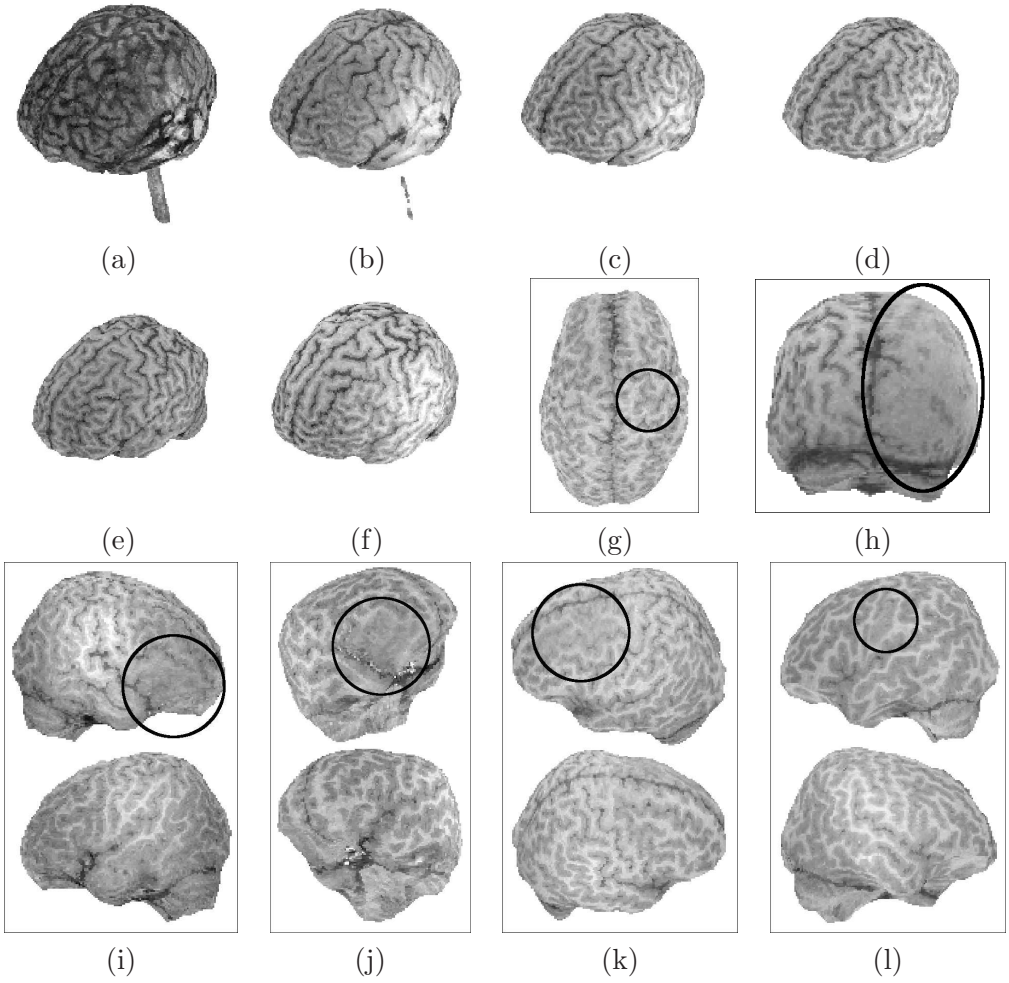

Figure 5: Examples of 3D renditions of the isosurfaces with voxel intensities. (a–d): Isosurface views of a same control subject at depths (a) 0mm, (b) 3mm, (c) 6mm and (d) 9mm. (e–f) Isosurface views at depth 5mm for two other controls. (g–l) Isosurface views with dysplastic lesions of 6 patients. (i–l) The opposite sides, with and without lesion, are shown for comparison. The depths are (g) 11.5mm, (h) 10.5mm, (i) 8mm, (j) 10.5mm, (k) 12mm, and (l) 10.5mm.

5 Conclusions

We presented a fully automatic approach to extract Euclidean isosurfaces of the human brain for the diagnosis of dysplastic lesions. The method exploits the topology of the forest

created by the IFT for brain segmentation (Fig. 4). It relies on gradient computation, detection of internal markers and leaking points on the object's border. The isosurfaces are computed using a 3D Euclidean distance transform of the resulting envelope of the brain and their visualization is finally used to assist the diagnosis of dysplastic lesions (Fig. 5). The method was successfully evaluated using 50 MR volumes (40 controls, 10 epilepsy patients with dysplastic lesions). The presented method for detection of leaking points is more elaborated than the one proposed by Falcão et. al [12] and worked correctly on all tested datasets. The resulting isosurfaces did not present the curvature artifacts that occur on the frontal and occipital lobes with the previous approach [1], currently available in [2].

Future research goals include I) evaluation of the leaking point selection algorithm for other applications; II) design of suitable gradient intensity functions faster than the one used here; and III) automatic detection of dysplastic lesions by exploiting the texture symmetry on the resulting isosurfaces of the brain.

Acknowledgments

This work was supported by CAPES, CNPq (proc. 302427/04-0) and FAPESP (proc. 03/13424-1).

References

[1] A. C. Bastos, R. M. Comeau, F. Andermann, D. Melanson, F. Cendes, F. Dubeau, S. Fontaine, D. Tampieri, and A. Olivier. Diagnosis of subtle focal dysplastic lesions: Curvilinear reformatting from three-dimensional magnetic resonance imaging. *Annals of Neurology*, 46(1):88–94, 1999.

[2] Rogue Research. BrainSight. http://www.rogue-research.com/B/epilepsy.htm.

[3] A.X. Falcão, J. Stolfi, and R.A. Lotufo. The image foresting transform: Theory, algorithms, and applications. *IEEE Trans. on Pattern Analysis and Machine Intelligence*, 26(1):19–29, 2004.

[4] E.R. Dougherty and R.A. Lotufo. *Hands-on Morphological Image Processing*. SPIE Press, Bellingham, WA, 2003.

[5] E.W. Dijkstra. A note on two problems in connexion with graphs. *Numerische Mathematik*, 1:269–271, 1959.

[6] L. Vincent and P. Soille. Watersheds in digital spaces: An efficient algorithm based on immersion simulations. *IEEE Trans. on Pattern Analysis and Machine Intelligence*, 13(6), Jun 1991.

[7] R.A. Lotufo and A.X. Falcão. The ordered queue and the optimality of the watershed approaches. In *Mathematical Morphology and its Applications to Image and Signal Processing*, volume 18, pages 341–350. Kluwer, Jun 2000.

[8] P. Felkel, M. Bruckschwaiger, and R. Wegenkittl. Implementation and complexity of the watershed-from-markers algorithm computed as a minimal cost forest. *Computer Graphics Forum (EUROGRAPHICS)*, 20(3):(C) 26–35, 2001.

[9] A.X. Falcão and F.P.G. Bergo. Interactive volume segmentation with differential image foresting transforms. *IEEE Trans. on Medical Imaging*, 23(9):1100–1108, 2004.

[10] J.K. Udupa and S. Samarasekera. Fuzzy connectedness and object definition: Theory, algorithms, and applications in image segmentation. *Graphical Models and Image Processing*, 58:246–261, May 1996.

[11] A.X. Falcão, L.F. Costa, and B.S. da Cunha. Multiscale skeletons by image foresting transform and its applications to neuromorphometry. *Pattern Recognition*, 35(7):1571–1582, 2002.

[12] A.X. Falcão, F.P.G. Bergo, and P.A.V. Miranda. Image segmentation by tree pruning. In *Proc. of the XVII Brazillian Symposium on Computer Graphics and Image Processing*, pages 65–71. IEEE, Oct 2004.

[13] O. Cuisenaire and B. Macq. Fast Euclidean distance transformation by propagation using multiple neighborhoods. *Computer Vision and Image Understanding*, 76(1):163–172, Nov 1999.

[14] C.R. Maurer Jr., R. Qi, and V. Raghavan. A linear time algorithm for computing exact Euclidean distance transforms of binary images in arbitrary dimensions. *IEEE Trans. on Pattern Analysis and Machine Intelligence*, 25(2):265–270, 2003.

[15] Bluevoxel Software. Bluevoxel Alberio. http://www.bluevoxel.com/alberio_en.php.